SAND2017-6200J

Coarse Grained Modeling of Polyethylene Melts: Effect on Dynamics

Brandon L. Peters,[1] K. Michael Salerno,[2] Anupriya Agrawal,[3] Dvora Perahia,[4] and Gary S. Grest[1]
[1)] *Sandia National Laboratories, Albuquerque, New Mexico, 87185, USA*
[2)] *U. S. Naval Research Laboratory, Washington, DC 20375, USA*
[3)] *Department of Mechanical Engineering and Materials Science, Washington University in St. Louis, Missouri 63130, USA*
[4)] *Department of Chemistry, Clemson University, Clemson, South Carolina 29634, USA*

(Dated: 9 May 2017)

The distinctive viscoelastic behavior of polymers results from a coupled interplay of motion on multiple length and time scales. Capturing the broad time and length scales of polymer motion remains a challenge. Using polyethylene (PE) as a model macromolecule, we construct coarse-grained (CG) models of PE with 3-5 methyl groups per CG bead and probe two critical aspects of the technique: pressure corrections required after iterative Boltzmann inversion (IBI) to generate CG potentials that match the pressure of reference fully-atomistic melt simulations and the transferability of CG potentials across temperatures. While IBI produces non-bonded pair potentials which give excellent agreement between the atomistic and CG pair correlation functions, the resulting pressure for the CG models is large compared to the pressure of the atomistic system. We find that correcting the potential to match the reference pressure leads to non-bonded interactions with much deeper minima and slightly smaller effective bead diameter. However, simulations with potentials generated by both IBI and pressure-corrected IBI result in similar mean-squared displacement (MSD) and stress auto correlation functions $G(t)$ for PE melts. While the time rescaling factor required to match CG and atomistic models is the same for pressure and non-pressure corrected CG models, it strongly depends on temperature. Transferability was investigated by comparing the MSD and $G(t)$ for potentials developed at different temperatures.

I. INTRODUCTION

Modeling dynamics of entangled polymers is challenging since the time for a polymer to diffuse its own size increases faster than N^3 where N is the polymerization number. Capturing dynamics is critical for the realization of the unique viscoelastic behavior of polymers. With typical N varying from tens to millions this time becomes exponentially greater than the shortest time scales, which are on the scale of the bond vibrations. As a result, fully atomistic simulations of entangled polymer liquids, even at temperatures far above the glass transition, remain computationally inaccessible. To overcome this limitation, coarse-grained (CG) models have been developed to study polymer dynamics on long time scales that capture their unique properties. The most basic CG model is the bead-spring description,[1] in which polymer chains are modeled simply by beads connected by a finite extensible spring to avoid chain crossing. Because of its simplicity and computational efficiency, this model has been widely used to probe phenomena that occur at long length and time scales.[1–4] To incorporate the local details, yet retain computational efficiency, new atomistic derived CG models have recently been developed.[5–8]

The basic approach of all atomistic derived CG models is to combine groups of atoms into pseudoatoms. United atom (UA) models,[9–13] which combine each CH_2/CH_3 group into a single pseudoatom, have been in use for decades. UA nonbonded interactions are often fit to a functional form, such as a Lennard-Jones (LJ) 12:6 or Buckingham exponential-6 potential, with parameters chosen to reproduce physical properties such as densities and critical temperatures of small molecules. Another widely used CG representation is the MARTINI model,[14] where each bead represents of order four CH_2/CH_3. In this model, the nonbonded interactions are assumed to be LJ 12:6 potentials with the interaction parameters fit to match bulk densities and compressibilities of short alkane chains. To improve the ad-hoc approach often used to determine the interaction parameters for UA and MARTINI potentials, more rigorous approaches such as force matching, iterative Boltzmann inversion, and optimized relative entropy have been developed.[15–21] These new powerful methods encode atomistic details into the CG model interactions, enabling simulation over extended length and time scales. While atomistic-derived CG models capture well some properties they are not yet universally derived and face several challenges that arise from the basic construction of the potentials.

One critical open question in developing CG models is determining the optimal number of atoms represented by a CG bead that enable effective measurements of the properties of the system.[22] This issue is directly correlated with resolving the shortest length scale in a polymer that is fundamental to the macroscopic dynamics and properties. Using linear polyethylene as a model system, we[23,24] have probed the effects of the degree of coarse-graining on structure and dynamics of highly entangled polymer melts. The number of -CH_2- methylene groups λ in a psuedoatom was varied as illustrated in Figure 1 and potentials were developed using IBI for $\lambda = 2-6$. This work showed that independent of the degree of coarse graining, all static and dynamic properties are essentially the same once the dynamic scaling factor

α and non-crossing constraint for $\lambda = 6$ are included.[23] Using this CG model we were able to reach times of over 500 μs, allowing us to measure a number of quantities which can be compared directly to experiments, including the stress relaxation function, plateau modulus and shear viscosity.[24] Here we build on this understanding of the CG process, resolving the pressure effects that arise from IBI methods and the temperature transferability of CG potentials.

Further, we show that the dynamic rescaling factor α, which results from the smoother free-energy landscape of the CG models[15,21,23,25–32] compared with atomistic ones increases with decreasing temperature. This allows one to reach even longer effective simulation times as temperature is reduced towards the glass transition temperature.

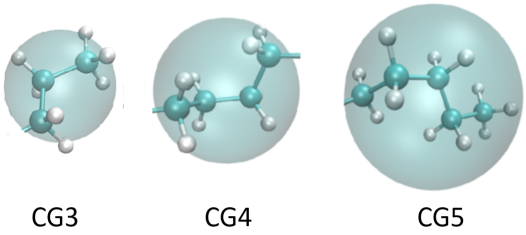

FIG. 1. Coarse grained bead for $\lambda = 3$, 4 and 5. The bead diameter corresponds to the position of the minimum in the nonbonded interaction.

II. MODEL AND METHODOLOGY

A. Atomistic and Coarse Grained Models

The CG models were derived from atomistic simulations of 345 chains of C_nH_{2n+2} with $n = 96$ for $\lambda = 3$, 4 and 6 and $n = 95$ for $\lambda = 5$. Figure 1 shows the CG beads for $\lambda = 3$, 4 and 5. CG models were derived at temperature T = 500 K, mass density $\rho = 0.72$ g/cm^3 and T = 400 K, $\rho = 0.77$ g/cm^3. The atomistic simulations used the All Atom Optimized Potentials for Liquid Simulations (OPLS-AA)[33,34] potential with modified dihedral coefficients that better reproduce the properties of long alkanes.[35] With this modified potential the mean-squared radius of gyration $\langle R_g^2 \rangle$ and end-to-end distance $\langle R^2 \rangle$ match experimental values.

Most simulations were run at constant volume with a Langevin thermostat with damping time constant t_v to maintain the temperature.[36,37] In the atomistic simulations, the nonbonded potential is the sum of LJ and long-ranged Coulomb interactions, while for the CG models the nonbonded potential is short-ranged. In the atomistic simulations the Langevin damping constant is $t_v = 1$ ps, while for the CG model $t_v = 10$ ps. For the atomistic simulations, the attractive r^{-6} dispersion term in the LJ

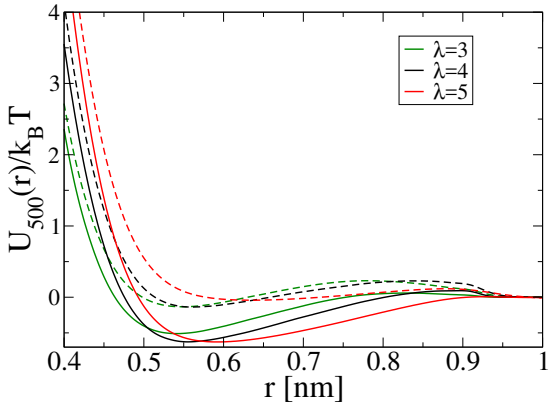

FIG. 2. Nonbonded potentials $U_{500}(r)$ for CG3 (green), CG4 (black) and CG5 (red) before (dashed) and after (solid) the pressure correction.

interaction and the electrostatic interactions are calculated using the particle-particle-particle-mesh (PPPM) algorithm.[38] Interactions closer than 1.2 nm are calculated in real space; those outside this range are calculated in reciprocal space with precision of 3x10^{-5}. The repulsive r^{-12} term in the LJ interaction is truncated at 1.2 nm. For the atomistic model, the bond, angle, dihedral and nonbonded interactions are integrated with a 1 fs time step, and long-ranged interactions are integrated with a 4 fs time step using the RESPA integrator.[39] For the CG models the nonbonded interactions are truncated at 1.0 nm. The time step for the CG simulations is 10 fs for $\lambda = 3$ and 20 fs for $\lambda \geq 4$. For CG6, we found that the maximum bond length is larger than the characteristic size of the CG bead and as a result, the chain cut through each other.[23,24] As a result for CG6 we adopted a modified segmental repulsive potential developed by Sirk *et al.*[40] to prevent chain crossing. All simulations are performed using the Large Atomic Molecular Massive Parallel Simulator (LAMMPS) molecular dynamics code.[41]

Atomistic C_nH_{2n+2} samples with $n = 96$ and $n = 95$ were first equilibrated at 400 and 500 K for 30 ns, after which particle configurations were sampled every 0.1 ns for 7 ns. Over this time the chains moved a significant distance relative to their end-to-end size, and many local conformations were sampled. Atomistic simulations for a system of 216 chains of length $n = 480$ were also run at 500 K at $\rho = 0.73$ g/cm^3 for 675 ns and at 400 K at $\rho = 0.77$ g/cm^3 for 2275 ns. Both the n=96 and 480 systems were used to calibrate the time scaling for the CG potentials. For $n = 96$ and $n = 95$, we ran also simulations at 450K, 550K, and 600K to calculate the dynamic scaling factor α.

The CG models use bond and angle distributions from the atomistic simulation to create a tabulated CG potential. The bond potential is calculated from the distribution of bond lengths $P(l)$,

$$U_B(l) = -k_B T \ln \left[P(l)/l^2 \right] \quad (1)$$

TABLE I. Pressure, density, and end-to-end distance $\langle R^2 \rangle$ for the simulations performed at 500K with $U_{500}(r)$.

n	CG model	$\langle R^2 \rangle$ $[nm^2]$	Pressure Corrected [MPa]	Non Pressure Corrected [MPa]	Density $[g/cm^3]$
96	AA	14.5 ± 0.6	2.0 ±2.5	-	0.72
	CG3	16.8 ±0.6	4.1 ±2.73	308.8 ±3.2	0.72
	CG4	17.7 ±0.7	5.2 ±1.21	241.0±2.4	0.72
	CG5	18.6 ±0.8	9.1 ±2.12	192.5±2.0	0.72
	CG6	15.4 ±1.0	4.2 ±0.98	124.5 ±1.3	0.72
480	AA	88.6 ±0.6	8.52 ±9.3	-	0.73
	CG3	94.4 ±0.6	14.4 ±2.03	329.8 ±1.7	0.73
	CG4	101.1 ±0.7	5.8 ±1.36	261.4±1.4	0.73
	CG5	109.8 ±0.8	9.5 ±1.05	169.0 ±1.1	0.73
1920	CG4	382.3 ±0.7	15.6 ±0.36	447.6 ±0.7	0.76
	CG5	360.9±0.8	12.7 ±0.30	203.3 ±0.3	0.76

where l is the bond length for CG beads overlaid on the atomistic reference configurations. The bond potentials for the CG models with CG3, CG4, and CG6 are shown in Salerno *et al.*[24] Similarly, the angle potential

$$U_A(\theta) = -k_B T \ln \left[P(\theta)/sin(\theta) \right] \tag{2}$$

is computed from the distribution $P(\theta)$, where θ is the angle between CG bead triplets from the atomistic reference configuration. The angle potentials $U_A(\theta)$ for $\lambda = 3$, 4 and 6 are shown in Salerno *et al.*[24] Both the bond and angle potentials were the same at 400 and 500 K. For the nonbonded tabulated potential $U_{NB}(r)$, we used IBI

$$U_{NB}^{i+1}(r) = U_{NB}^{i}(r) + \Lambda k_B T \ln \left[\frac{g^i(r)}{g(r)} \right] \tag{3}$$

where $g(r)$ is the target intermolecular radial distribution function obtained from the atomistic simulation and $g^i(r)$ is the radial distribution function of the current iteration i. The initial potential, $U_{NB}^0(r) = -k_B T \ln [g(r)]$. During the iteration procedure $\Lambda = 0.5$ initially, but Λ is tuned as $g^i(r)$ converges toward the target $g(r)$. The potential and force are required to go smoothly to zero at the cutoff by multiplying the potential by the Mei-Davenport-Fernando taper function.[42]

$$f(x) = \begin{cases} 1, & r \le r_m \\ (1-x)^3(1+3x+6x^2), & r_m \le r \le r_c \\ 0, & r_c \le r \end{cases} \tag{4}$$

where $x = (r - r_m)/(r_c - r_m)$, $r_m = 0.9$ nm is the start of the taper range and r_c is the cut off distance. After 50−70 iterations, the radial distribution nicely converges to the target $g(r)$ as shown in Figure 3 for $T = 500$ K, giving the resulting nonbonded potential shown in Figure 2 by the dashed lines. However, the resulting pressure P of all four of the resulting CG model is large, a seen in Table I.

This pressure enhancement has been observed in IBI generated CG potentials and to reduce the pressure of the CG models to better match that of the atomistic system, pressure correction has been applied[43–45]

$$\Delta U_{pc}^{i+1} = -\left(P_i - P\right) V_0 \gamma \left(1 - \frac{r}{r_c}\right) \tag{5}$$

where P_i is the average pressure during iteration i, $P = 3$ MPa is the target pressure, and γ is a factor to control convergence.

B. Pressure Effects and Transferability

Pressure Correction Effects While application of the IBI procedure to extract the non-bonded potential leads to excellent agreement between the target $g(r)$ and that for the CG model for all λ, the resulting CG system often has unrealistic high pressures. There are two ways to address it. The first is to disregard the excess pressure and run constant volume simulations at experimental densities. We will further discuss this approach as our new potentials are applied to polymers. The second is to apply a pressure correction.[43–45]

The pressure correction was applied with an additional 10−20 IBI iterations, generating pressure corrected nonbonded potentials, with pressures much lower than before the pressure corrections as shown in Table 1. The resulting nonbonded potentials are shown by the solid lines in Figure 2 for $T = 500$ K. Pressure corrected, each nonbonded potential has a deeper minimum, and a slightly smaller effective diameter compared to non-pressure corrected ones. Reducing the pressure of the CG model increases the height of first peak in the radial distribution function, as seen in Figure 3. We refer to these nonbonded potentials developed at 500 K as $U_{500}(r)$.

Temperature transferability Here we test the transferability of the potentials developed for $\lambda = 4$. In Figure 4, the target radial distribution function for $C_{96}H_{194}$ at 400 K, $\rho = 0.77$ g/cm^3 is compared to the the pressure corrected

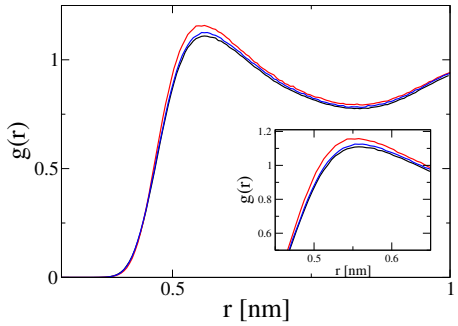

FIG. 3. Intermolecular radial distribution function g(r) for the atomistic $C_{96}H_{194}$ system (black) compared to CG4, before (blue) and after (red) the pressure correction at $T = 500$ K. Inset shows the region around the first peak.

CG potential $U_{400}(r)$. The pressure for the IBI potential without the pressure correction is 280 MPa. As for 500 K, the pressure corrected potential produces a slight increase in the height of the first peak compared to the target. For comparison, $g(r)$ for the pressure corrected CG $U_{500}(r)$ run at 400 K at the same density is shown. As seen in Figure 5, the attractive well is 20% deeper for CG potential developed at 500 K compared to that at 400. (Note that the potential in Figure 5 is normalized by the k_BT.) The position of the minimum is shifted only slightly from $r_{\min} = 0.552$ nm for $U_{500}(r)$ to 0.548 nm for $U_{400}(r)$.

Comparing the pressure corrected $U_{500}(r)$ to the standard LJ 12:6 potential, which is often used in bead-spring models of polymers,[1–4] show that these atomistically inspired CG potentials are softer with a much shallower attractive well than the LJ 12:6 potential. Since PE is locally stiff, as the degree of coarse graining increases, the methyl groups in each CG bead take up less of the volume. As a result, the nonbonded potentials become softer with increasing λ. A similar softening of the potential with increasing degree of coarse graining was found by Clark *et al.*[46] who represented each chain as a collection of interpenetrating blobs. This effect is seen in Figure 5 where the CG models, already softer than the LJ potential, are progressively softer as λ increases.

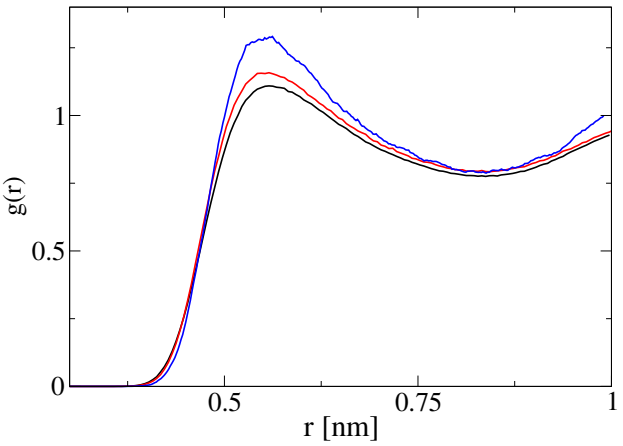

FIG. 4. Intermolecular radial distribution function g(r) for the atomistic $C_{96}H_{194}$ system (black) and for CG4 for $U_{400}(r)$ (red) and $U_{500}(r)$ (blue) at 400 K.

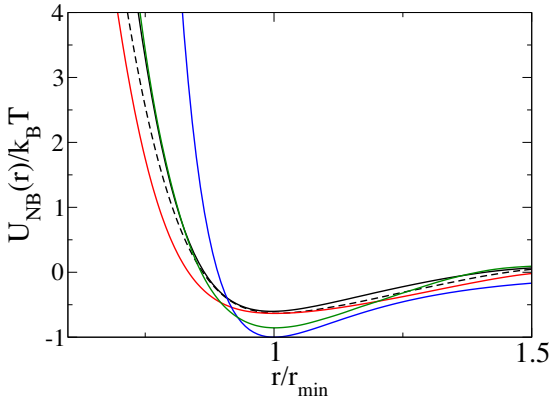

FIG. 5. Pressure corrected non-bonded potentials $U_{NB}(r)$ generated at 400 K (black solid) and 500 K (black dashed) for $\lambda = 4$ and at 500 K for CG5 (red) and CG3 (green) compared to LJ $12:6$ interaction (blue). The distance is scaled by the position of the attractive minimum $r_{\min}$ and the strength of the potential is scaled by k_BT for the PE models and ϵ for the LJ potential.

III. APPLICATION OF POTENTIALS TO POLYMERS

A. Effects of Pressure Correction

As was shown in the previous section, introducing a pressure correction that uses the atomistic pressure as a guide, results in the pair correlation function $g(r)$ for the CG system that slightly diverges from the target. However, we find that these difference hardly leads to any variances in the static properties of the system, including the end-to-end distant, radius of gyration and single chain structure factor $S(q)$[23,24]. The impact on polymer dynamics was further explored. It is now well established that coarse graining reduces the number of degrees of freedom in a system, creating a smoother free-energy landscape compared with fully atomistic simulations. This results in faster dynamics for the polymer chain than for the fully atomistic model.[15,21,23,25–32]

The dynamics of the atomistic and CG models can be mapped on to each other by scaling time in the CG models by a dynamic scaling factor α.[15,21,23,25–32] We have previously shown that for the pressure corrected potentials, α is dependent on the degree of coarse graining λ, but α does not depend on chain length, at least for $n \geq 96$.[23,24] Here, to determine the effects of including the pressure correction on the chain mobility we follow

the MSD of the inner 6 CG beads $g_1(t)$ for systems prepared using the pressure and non-pressure corrected potentials for $\lambda = 4$ at 500 K and compared it to the mobility of the inner 24 CH_2 beads for the atomistic model for $n = 96$ and 480. As seen in Figure 6, $g_1(t)$ for the atomistic and both CG models collapse onto the same curve after scaling time by α. α is essentially same for the pressure and non-pressure corrected potentials for all λ studied as seen from the inset, even though the well depth of the two are significantly different. This result is consistent with that of Grest[4] who showed that at fixed density, far above the glass transition the depth of the attractive well has little effect on the chain mobility.

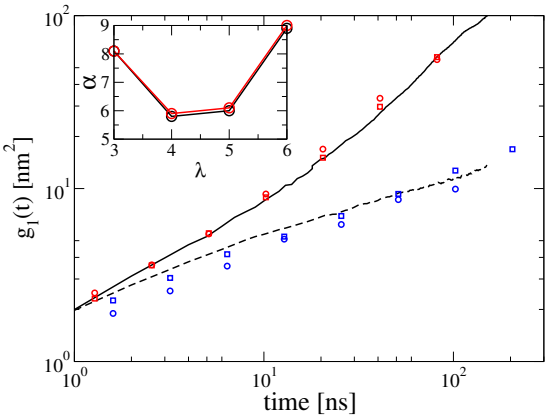

FIG. 6. Mean squared displacement $g_1(t)$ of the center 24 carbons for C_nH_{2n+2} atomistic model for $n = 96$ (solid line) and $n = 480$ (dashed line) compared to that of the center 6 CG beads for the pressure corrected (circles) and non-pressure corrected (squares) CG model for $n = 96$ (red) and $n = 480$ (blue) for CG4 at 500 K. The data for the CG models are scaled by α in time so that they overlap with the atomistic results. Inset: α versus λ at 500 K, with (black) and without (red) the pressure correction.

As much of the fascinating dynamics of polymers is in their entangled regime, MSD of entangled chains for the two potentials is probed. The MSD of the center of mass $g_3(t)$ and $g_1(t)$ for the inner 6 beads for $C_{1920}H_{3842}$ for the pressure and non-pressure corrected potentials for CG4 and 5 are compared in Figure 7. There is no noticeable difference between the two potentials or for the degrees of coarse graining. As discussed previously,[23,24] the $g_1(t)$ of inner monomers shows a distinct crossover from the early time $t^{1/2}$ Rouse regime to $t^{1/4}$ intermediate scaling predicted by the tube model at an entanglement time $\tau_e \sim 10$ ns. For late times, as shown in Figure 7, the MSD of the center of mass and inner monomers converge at a diffusive time $\tau_d \sim 10^5$ ns with a diffusion coefficient $D = 1.2 \times 10^{-12}$ m^2/s for $n = 1920$. These results for the intermediate $t^{1/4}$ power law are in good agreement with previous long time simulations using the bead-spring model.[1,3] However, unlike the bead-spring model this result demonstrates that one can capture long time and length scales while accounting for atomistic details.

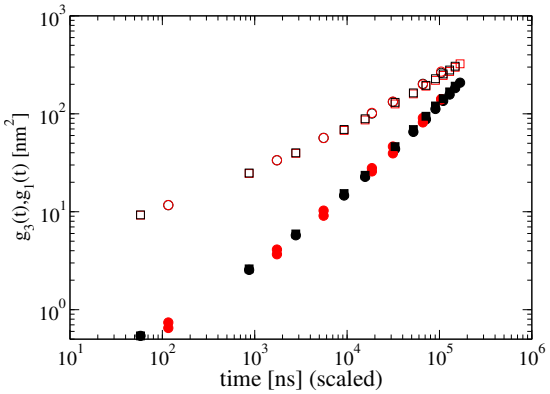

FIG. 7. MSD for the center of mass $g_3(t)$ (closed) and inner 6 monomers $g_1(t)$ (open) for $C_{1920}H_{3842}$ at 500 K for CG4 (squares) and CG5 (circles) for pressure corrected (black) and non-pressure corrected (red)

.

The stress response is one of the unique properties of polymers that characterize their viscoelastic behavior. The stress response function after a small perturbation $G(t)$ can be expressed by the stress autocorrelation function according to the fluctuation-dissipation theorem, $G(t) = (V/k_BT)\langle\sigma_{\alpha\beta}(t)\sigma_{\alpha\beta}(0)\rangle$ where $\sigma_{\alpha\beta}(t)$ are the off-diagonal components $\langle xy\rangle$, $\langle xz\rangle$ and $\langle yz\rangle$ of the stress tensor. For all degrees of coarse graining and chain lengths we studied, we found little difference between the pressure and non-pressure corrected potentials. As shown in Salerno *et al.*[24], for CG4, for example, the plateau value $G_0^N = 2.1 \pm 0.3$ MPa and entanglement molecular weight $M_e = \rho RT/G_0^N = 1300$ g/mol are in good agreement with experiment.[47–49] A similar plateau modulus value was found by Padding and Briels[50] for $n = 1000$ with $\lambda = 20$ with their non-crossing constraint.

Next, we calculated the bulk modulus for the atomistic and CG4 pressure and non-pressure corrected models at 500K. The simulation cell was compressed at a constant rate of 6.66x10^{-4} m/s for the atomistic simulations. The CG simulations were compressed at the same scaled rate. The pressure corrected bulk modulus 576 MPa is similar to that obtained for the atomistic model, 653 MPa, while the bulk modulus for the non-pressure corrected potential as much higher, 1085MPa. This result is in contrast to Wang *et al.*[45] who found for water their pressure corrected gave a modulus which significantly deviated from that obtained using atomistic models.

The difference in the two potentials is most strongly seen when varying the temperature. One example is the thermal expansion coefficient. In this case we slowly cooled the $C_{96}H_{194}$ melt from 500 K to 200K at constant pressure. For the non-pressure corrected potential, we held the pressure at $P = 241$ MPa, its value at 500 K. For the pressure corrected potential we set $P = 3$ MPa. As shown in Figure 8, the agreement between the atomistic and two pressure corrected potentials for the density

as a function of temperature is in reasonably good agreement while the thermal expansion is clearly much lower than the atomistic simulation for non-pressure corrected potential. The linear thermal expansion coefficients at 480 K are 3.5 and 3.6 x 10^{-4} g/cm^3K for the pressure corrected potentials $U_{500}(r)$ and $U_{400}(r)$ and 1.6 x 10^{-4} g/cm^3K for the non-pressure corrected $U_{500}(r)$ potential compared with 3.1 x 10^{-4} g/cm^3K for the atomistic model. The pronounced density increase between 230 and 300 K corresponds to a semicrystalline state.

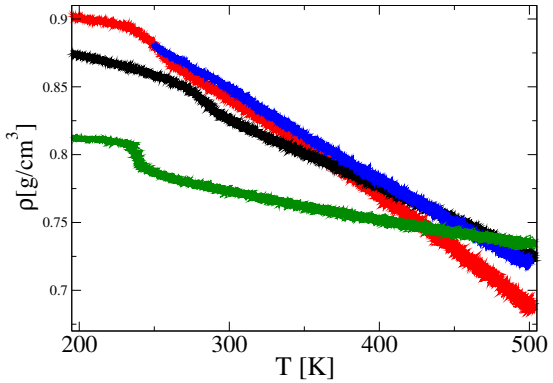

FIG. 8. Density versus temperature for the atomistic simulation for $C_{96}H_{194}$ (blue) and for CG4 pressure (black) and non-pressure corrected potential (green) for $U_{500}(r)$ and the pressure corrected potential $U_{400}(r)$ (red) cooled at 0.0875 K/ns. For the CG models, the time is unscaled.

B. Transferability of the Potential

One of the main unsettled issues with the wide use of CG potentials is the transferability between temperatures. Moore *et al.*[51], used multiple temperatures to develop their CG potential for a generic LJ fluid and mutliple small molecules, but did not explore the pressure, thermodynamics, nor the dynamics. We have developed two potentials at 400 and 500 K. As seen in Figure 5 while the position of the potential minimum is only slightly shifted for the CG nonbonded potential developed at 500 K compared to 400 K, the depth of the attractive well is 20% deeper for CG potential developed at 500 K compared to that at 400 K. This results in an 10% increase in the height of first peak for the pair correlation function $g(r)$ for $U_{500}(r)$ compared to $U_{400}(r)$ when both are used at T = 400 K as shown in Figure 4. The measured end-to-end distance and radius of gyration was essentially the same for the two potentials when run at 400 K. To test the impact of this difference in the non-bonded potential on the dynamics, we compare in Figure 9, the MSD of the center of mass $g_3(t)$ and that of the center 6 beads $g_1(t)$ for the potentials. Even though the well depth of the two potentials are significantly different, they give very similar dynamics.

As a further test, we determined the stress autocorrelation function $G(t)$ at 400 K for the potentials derived at 400 and 500 K but run at $T = 400$ K. As shown in Figure 10, the plateau of $U_{400}(r)$ is a little lower than $U_{500}(r)$. The plateau value $G_0^N = 2.0 \pm 0.3$ MPa and entanglement molecular weight $M_e = \rho RT/G_0^N = 1500 \pm 200$ g/mol for $U_{500}(r)$, and $G_0^N = 1.6 \pm 0.3$ MPa and $M_e = 1700 \pm 300$ g/mol for $U_{400}(r)$.

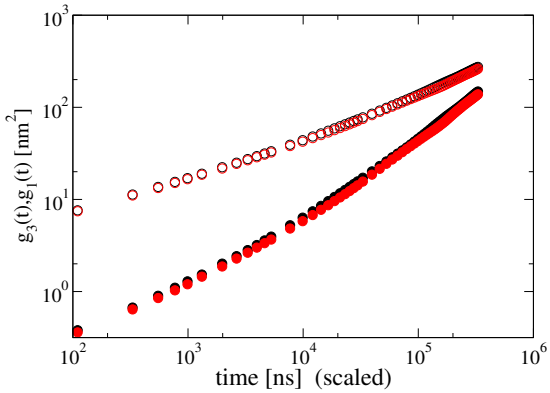

FIG. 9. Mean squared displacement of the center of mass $g_3(t)$ (closed) and center beads $g_1(t)$ (open) for $n = 1920$ for $U_{400}(r)$ (red) and $U_{500}(r)$ (black) at 400K for CG4.

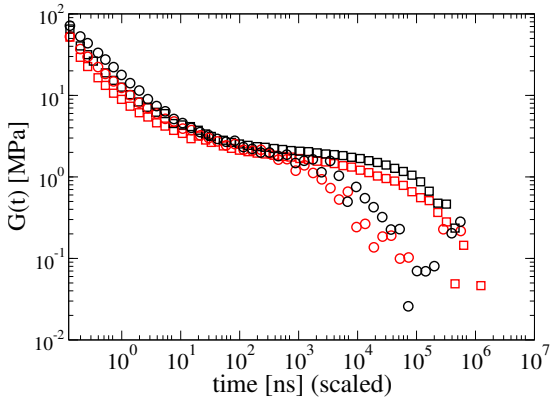

FIG. 10. Stress autocorrelation function $G(t)$ for CG4 at $400K$ for $U_{400}(r)$ (red) and $U_{500}(r)$(black) for $n = 480$ (circles) and for $n = 1920$ (squares).

One of the advantages of using CG models is that the dynamics can be considerably faster than for the atomistic models while retaining atomistic details. For PE the dynamic scaling factor α between the atomistic and CG models varies from a factor of 6 to 9 at $T = 500$K depending on the degree of coarse graining as shown in the inset of Figure 6. Not surprisingly, the dynamic scaling factor α is temperature dependent as shown in Figure 11 for CG4 and CG5. α is only weakly temperature dependent for high $T \geq 500$ K but increases to $\sim$ 12 at 400 K for both degrees of coarse graining. As seen in the inset, α follows the Vogel-Fulcher equation $\alpha = \alpha_0 exp(A/(k(T - T_{VF})))$ with $\alpha_0 = 4.126$, $A/k = 80.33$, and $T_{VF} = 324.83$.[52] Further, we show

that the dynamic rescaling factor, which results from the smoother free-energy landscape of the CG models compared with atomistic ones increases with decreasing temperature.[52] This increase in α as T decreases can be very advantageous in modeling entangled polymers near the glass transition as relaxation times diverge exponentially. Combining the larger time step and reduced number of degrees of freedom for the CG models with dynamic rescaling factor, allows one to reach effective simulation times not possible using fully atomistic models.

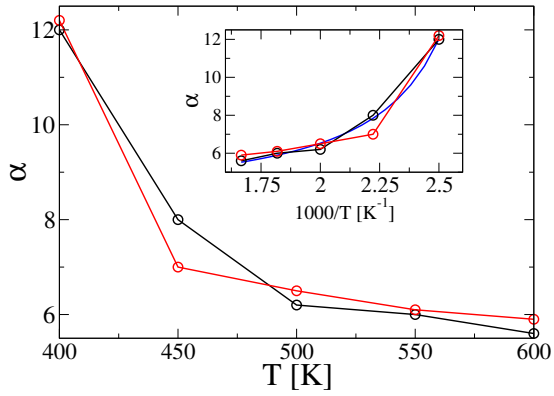

FIG. 11. Scaling factor α for $U_{500}(r)$ for CG4 (red) and CG5 (black) versus temperature. The inset shows the same data plotted versus $1000/T$ with the Vogel-Fulcher equation (blue).

IV. SUMMARY

Here we have shown the physical implications of pressure corrections in atomistic derived CG models and their effect on polymer dynamics. Using PE as a model system we showed that while the IBI method produced non-bonded pair potentials which give excellent agreement for the atomistic and CG pair correlation functions, the resulting pressure for all degrees of coarse graining studied is very large. Correcting the potential so the pressure P ~ 0 leads to non-bonded models with much deeper minimum and slightly smaller effective diameter. However, both the pressure and non-pressure corrected CG models give similar results for the mean squared displacement and the stress auto correlation function for PE melts when run at the same density. The pressure correction does not change the time rescaling factor α between the CG models and the atomistic model. The difference in the two potentials does affect strongly the thermal expansion, with the pressure corrected potential in better agreement with the atomistic simulation than the non-pressure corrected potential.

As one of the current limitations of using CG models is the transferability of the pair potentials, we developed CG potentials at different temperatures. We find, the depth of the attractive well in the non-bonded pair potential decreases as the reference temperature used to develop the CG potential decreases. While the decrease in the well depth results in differences in the height of the first peak in the pair correlation function, somewhat surprisingly, there was little effect on the chain mobility or viscoelastic response.

Finally, we showed that the dynamic rescaling factor α is essentially the same for the IBI and pressure-corrected IBI potentials for a fixed density and temperature. This is consistent with the idea that coarse graining reduces the number of degrees of freedom, creating a smoother free-energy landscape compared with fully atomistic simulations. As the temperature decreases and density increases, the local packing inhibits the motion of the atomistic system more so than that of the soft CG beads, resulting in an increase in α.

V. ACKNOWLEDGEMENTS

DP acknowledge financial support from Grant No. DMR-1611136. This work was supported by the Sandia Laboratory Directed Research and Development Program. Research was carried out in part, at the Center for Integrated Nanotechnologies, a U.S. Department of Energy, Office of Basic Energy Sciences user facility. Sandia National Laboratories is a multimission laboratory managed and operated by National Technology and Engineering Solutions of Sandia, LLC., a wholly owned subsidiary of Honeywell International, Inc., for the U.S. Department of Energys National Nuclear Security Administration under contract DE-NA-0003525.

[1]Kremer, K.; Grest, G. S. *J. Chem. Phys.* **1990**, *92*, 5057–5086.
[2]Kremer, K.; Grest, G. S. In *Monte Carlo and molecular dynamics simulations in polymer science*; Binder, K., Ed.; Oxford University Press: New York, 1995; pp 194–271.
[3]Hsu, H.-P.; Kremer, K. *J. Chem. Phys.* **2016**, *144*.
[4]Grest, G. S. *J. Chem. Phys.* **2016**, *145*, 141101.
[5]Müller-Plathe, F. *Chem. Phys. Chem.* **2002**, *3*, 754–769.
[6]Nielsen, S. O.; Lopez, C. F.; Srinivas, G.; Klein, M. L. *J. Phys. Condens. Mat.* **2004**, *16*, R481.
[7]Peter, C.; Kremer, K. *Soft Matter* **2009**, *5*, 4357–4366.
[8]Li, Y.; Abberton, B. C.; Kröger, M.; Liu, W. K. *Polymers* **2013**, *5*, 751.
[9]Paul, W.; Yoon, D. Y.; Smith, G. D. *J. Chem. Phys.* **1995**, *103*, 1702–1709.
[10]Mondello, M.; Grest, G. S. *J. Chem. Phys.* **1995**, *103*, 7156–7165.
[11]Nath, S. K.; Escobedo, F. A.; de Pablo, J. J. *J. Chem. Phys.* **1998**, *108*, 9905–9911.
[12]Martin, M. G.; Siepmann, J. I. *J. Phys. Chem. B* **1998**, *102*, 2569–2577.
[13]Martin, M. G.; Siepmann, J. I. *J. Phys. Chem. B* **1999**, *103*, 4508–4517.
[14]Marrink, S. J.; Risselada, H. J.; Yefimov, S.; Tieleman, D. P.; de Vries, A. H. *J. Phys. Chem. B* **2007**, *111*, 7812–7824.
[15]Müller-Plathe, F. *ChemPhysChem* **2002**, *3*, 754–769.
[16]Reith, D.; Pütz, M.; Müller-Plathe, F. *J. Comput. Chem. 24*, 1624–1636.
[17]Izvekov, S.; Voth, G. A. *J. Phys. Chem. B* **2005**, *109*, 2469–2473.
[18]Shell, M. S. *J. Chem. Phys.* **2008**, *129*, 144108.
[19]Rühle, V.; Junghans, C. *Macromolecular Theory and Simulations* **2011**, *20*, 472–477.
[20]Noid, W. *J. Chem. Phys.* **2013**, *139*, 09B201.

[21]Guenza, M. *The European Physical Journal Special Topics* **2015**, *224*, 2177–2191.
[22]McCarty, J.; Clark, A.; Copperman, J.; Guenza, M. *The Journal of chemical physics* **2014**, *140*, 204913.
[23]Salerno, K. M.; Agrawal, A.; Perahia, D.; Grest, G. S. *Phys. Rev. Lett.* **2016**, *116*, 058302.
[24]Salerno, K. M.; Agrawal, A.; Peters, B. L.; Perahia, D.; Grest, G. S. *European Physical Journal Special Topics* **2016**, *225*, 1707–1722.
[25]Depa, P. K.; Maranas, J. K. *J. Chem. Phys.* **2005**, *123*, 094901.
[26]Izvekov, S.; Voth, G. A. *J. Chem. Phys.* **2006**, *125*, 151101.
[27]Harmandaris, V. A.; Kremer, K. *Soft Matter* **2009**, *5*, 3920–3926.
[28]Harmandaris, V. A.; Kremer, K. *Macromolecules* **2009**, *42*, 791–802.
[29]Depa, P.; Chen, C.; Maranas, J. K. *J. Chem. Phys.* **2011**, *134*, 014903.
[30]Lyubimov, I. Y.; McCarty, J.; Clark, A.; Guenza, M. G. *J. Chem. Phys.* **2010**, *132*, 224903.
[31]Fritz, D.; Koschke, K.; Harmandaris, V. A.; van der Vegt, N. F. A.; Kremer, K. *Phys. Chem. Chem. Phys.* **2011**, *13*, 10412–10420.
[32]Lyubimov, I. Y.; Guenza, M. G. *J. Chem. Phys.* **2013**, *138*, 12A546.
[33]Jorgensen, W. L.; Madura, J. D.; Swenson, C. J. *J. Am. Chem. Soc.* **1984**, *106*, 6638–6646.
[34]Jorgensen, W. L.; Maxwell, D. S.; Tirado-Rives, J. *J. Am. Chem. Soc.* **1996**, *118*, 11225–11236.
[35]Siu, S. W. I.; Pluhackova, K.; Böckmann, R. A. *J. Chem. Theory Comput.* **2012**, *8*, 1459–1470.
[36]Schneider, T.; Stoll, E. *Phys. Rev. B* **1978**, *17*, 1302–1322.
[37]Grest, G. S.; Kremer, K. *Phys. Rev. A* **1986**, *33*, 3628–3631.
[38]Isele-Holder, R. E.; Mitchell, W.; Ismail, A. E. *J. Chem. Phys.* **2012**, *137*, 174107.
[39]Tuckerman, M.; Berne, B. J.; Martyna, G. J. *J. Chem. Phys.* **1992**, *97*, 1990–2001.
[40]Sirk, T. W.; Slizoberg, Y. R.; Brennan, J. K.; Lisal, M.; Andzelm, J. W. *J. Chem. Phys.* **2012**, *136*, 134903.
[41]Plimpton, S. *J. Comput. Phys.* **1995**, *117*, 1 – 19.
[42]Mei, J.; Davenport, J. W.; Fernando, G. W. *Phys. Rev. B* **1991**, *43*, 4653–4658.
[43]Milano, G.; Müller-Plathe, F. *J. Phys. Chem. B* **2005**, *109*, 18609–18619.
[44]Sun, Q.; Faller, R. *Computers & Chemical Engineering* **2005**, *29*, 2380 – 2385, Selected Papers Presented at the Symposium on Modeling of Complex ProcessesSymposium on Modeling of Complex ProcessesEngineering.
[45]Wang, H.; Junghans, C.; Kremer, K. *Euro. Phys. J. E* **2009**, *28*, 221–229.
[46]Clark, A. J.; McCarty, J.; Lyubimov, I. Y.; Guenza, M. G. *Physical review letters* **2012**, *109*, 168301.
[47]Vega, J. F.; Rastogi, S.; Peters, G. W. M.; Meijer, H. E. H. *J. Rheol.* **2004**, *48*, 663–678.
[48]Fetters, L. J.; Lohse, D. J.; Richter, D.; Witten, T. A.; Zirkel, A. *Macromolecules* **1994**, *27*, 4639–4647.
[49]Fetters, L. J.; Lohse, D. J.; Milner, S. T.; Graessley, W. W. *Macromolecules* **1999**, *32*, 6847–6851.
[50]Padding, J. T.; Briels, W. J. *J. Chem. Phys.* **2002**, *117*, 925–943.
[51]Moore, T. C.; Iacovella, C. R.; McCabe, C. *J. Chem. Phys.* **2014**, *140*, 224104.
[52]Fritz, D.; Herbers, C. R.; Kremer, K.; van der Vegt, N. F. *Soft Matter* **2009**, *5*, 4556–4563.